Advances in Cancer Biology - Metastasis 7 (2023) 100091

Contents lists available at ScienceDirect

Advances in Cancer Biology - Metastasis

journal homepage: www.journals.elsevier.com/advances-in-cancer-biology-metastasis

Partial EMT and associated changes in cellular plasticity in oncovirus-positive samples

Manas Sehgal [a,2], Ritoja Ray [a,1,2], Joel Markus Vaz [b], Shrihar Kanikar [c], Jason A. Somarelli [d], Mohit Kumar Jolly [b,*]

[a] Dr. D. Y. Patil Biotechnology and Bioinformatics Institute, Pune, India
[b] Centre for BioSystems Science and Engineering, Indian Institute of Science, Bangalore, India
[c] Indian Institute of Science Education and Research (IISER) Pune, Pune, India
[d] Department of Medicine and Duke Cancer Institute, Duke University, Durham, USA

ARTICLE INFO

Keywords:
Oncovirus
EMT
PD-L1
Metabolic reprogramming
Oxidative phosphorylation
Fatty acid metabolism
Glycolysis

ABSTRACT

Oncoviruses exploit diverse host mechanisms to survive and proliferate. These adaptive strategies overlap with mechanisms employed by malignant cells during their adaptation to dynamic micro-environments and for evasion of immune attack. While the role of individual oncoviruses in mediating cancer progression has been extensively characterized, little is known about the common gene regulatory features of oncovirus-induced cancers. Here, we focus on defining the interplay between several cancer hallmarks, including Epithelial-Mesenchymal Transition (EMT), metabolic alterations, and immune evasion across major oncoviruses by examining publicly available transcriptomics datasets containing both oncovirus-positive and oncovirus-negative samples. We observe that oncovirus-positive samples display varying degrees of EMT and metabolic reprogramming. While the progression of EMT generally associated with an enriched glycolytic metabolic program and suppressed fatty acid oxidation (FAO) and oxidative phosphorylation (OXPHOS), partial EMT correlated well with glycolysis. Furthermore, oncovirus-positive samples had higher activity and/or expression levels of immune checkpoint molecules, such as PD-L1, which was associated with a partial EMT program. These analyses thus decode common pathways in oncovirus-positive samples that may be used in pinpointing new therapeutic vulnerabilities for cancer cell plasticity.

1. Introduction

Oncoviruses are a class of viruses that can induce cancer in the host organism. A few examples of oncoviruses include the Epstein-Barr virus (EBV), human papillomavirus (HPV), hepatitis B virus (HBV), and hepatitis C virus (HCV). These can be primarily classified as DNA tumor viruses (HPV, HBV, and EBV) and RNA tumor viruses (HCV) [1]. Such viral infections can contribute to as high as 15% of human cancers worldwide [2]. Different oncoviruses are associated with specific cancer types; for example, HPV has been implicated in breast, skin, lung, cervical, and prostate cancer [1,3–5], while HBV and HCV are strong risk factors for hepatocellular carcinoma [6]. While an oncovirus infection does not always lead to cancer, chronic viral infections, paired with additional host factors, such as genomic instability, cell proliferation, and a milieu of genetic and epigenetic modifications, can ultimately initiate tumorigenesis [7].

A commonly observed phenomenon in cancer progression, which often associates with the remodeling of the tumor microenvironment, is epithelial-mesenchymal transition (EMT). EMT is a process that involves epithelial cells losing their epithelial traits, such as cell-cell adhesion and apico-basal polarity. Also, these cells gain migratory and invasive features often observed in a mesenchymal phenotype [8]. Partial or full EMT can be considered as a fulcrum of cancer cell plasticity; it is associated with multiple changes to cancer cell behavior, including migration and invasion, metabolic reprogramming, and immune evasion [9–15]. EMT in cancer is mediated by a host of tumor microenvironment factors, including hypoxia, matrix stiffness and crosstalk with other stromal cells [16–18]. In addition to these factors, oncoviruses are also

* Corresponding author.
E-mail address: mkjolly@iisc.ac.in (M.K. Jolly).
[1] Current address: Krieger School of Arts and Sciences, Johns Hopkins University, Baltimore, MD, USA.
[2] Equal contribution.

https://doi.org/10.1016/j.adcanc.2023.100091
Received 20 August 2022; Received in revised form 15 December 2022; Accepted 30 January 2023
Available online 2 February 2023

capable of inducing EMT in cancer cells. In 1994, Gilles and colleagues confirmed EMT and increased invasiveness in HPV33-infected cervical keratinocytes [19]. Since then, several studies have demonstrated the induction of EMT by major oncoviruses [20]. However, recent analyses have highlighted the spectrum of phenotypes observed along the epithelial/mesenchymal axis. Rather than a binary and complete switch to the mesenchymal state, cancer cells often display a mix of epithelial and mesenchymal traits, attaining one or more hybrid epithelial/mesenchymal (E/M) phenotypes [21]. Thus, this more complex and nuanced understanding of epithelial-mesenchymal plasticity prompts a renewed analysis of the association between oncoviruses and EMT-like phenotypes.

Another consequence of oncovirus infection is the reprogramming of host cell metabolism. Oncoviruses can rewire host cell metabolism to synthesize macromolecules important for both viral replication and tumor growth [22,23]. Such reprogramming is observed across many oncoviruses, although the degree to which this phenomenon occurs varies based on host factors and viral requirements. This reprogramming may also contribute to promoting cancer progression [24]. Hence, therapeutic solutions targeting specific metabolic pathways are likely to prevent viral infections and potential oncogenesis.

Besides the association between EMT and metabolic reprogramming, oncoviruses are also observed to interact with the host immune system. Many oncoviruses, such as EBV and HPV, are associated with increased levels of PD-L1, a co-inhibitor of cytotoxic T-lymphocyte attack [25]. Tumor cells expressing high PD-L1 are capable of evading T-cell-mediated anti-tumor responses [26]. Cells in partial or full EMT states often have higher levels of PD-L1 than epithelial ones [12,14], suggesting that EMT can contribute to immune evasion by upregulating immune checkpoints. However, it remains to be investigated whether oncoviruses induce an increase in PD-L1 and other checkpoints and whether this alteration in immune checkpoints is associated with a partial or full EMT.

Given the key connections between oncoviruses, EMT, metabolic plasticity, and immune evasion, we sought to better understand the coupling among these axes of plasticity in oncovirus-positive samples. To do this, we performed a comprehensive meta-analysis involving multiple human oncoviruses to analyze their associations with EMT, metabolic plasticity, and PD-L1 levels and activity using 80 transcriptomic datasets containing both oncovirus-positive and oncovirus-negative samples (Table S9). Our meta-analysis shows that oncovirus-positive samples often associate with a partial EMT, downregulation of oxidative phosphorylation and fatty acid oxidation metabolic pathways, and upregulation in glycolysis. Moreover, expression levels of *CD274* (gene encoding PD-L1) and activity for the PD-L1 pathway, together with expression levels of immune checkpoint molecules, such as *CD47*, *HAVCR2* and *CD276*, are enriched in oncovirus-positive samples. Thus, our results suggest a partial EMT phenotype and associated changes in metabolic reprogramming and T-cell-mediated immune checkpoints in the oncovirus-positive samples.

2. Materials and methods

2.1. Software and datasets

For computational and statistical analyses, Python (version 3.10) and R (version 4.1.2) were used. Microarray/RNA-sequencing datasets were downloaded from the National Center for Biotechnology Information Gene Expression Omnibus (NCBI GEO). For microarray datasets, probe-wise expression matrices were downloaded using GEOquery R Bioconductor package, and their corresponding annotation files were used to map probes to obtain the gene-wise expression. If more than one probe was mapped to the same gene, we used the average expression value of all probes mapped to that particular gene. The gene expression data was then log2-transformed (normalized). For RNA-seq datasets, sample-wise raw counts for each dataset (denoted by GSE ID) were downloaded from the NCBI GEO database, normalized for gene length, and transformed to TPM (transcripts-per-million) values which were then log2-transformed to obtain the final expression values for each gene per sample.

2.2. EMT, PD-L1, and metabolic scoring metrics

Epithelial-mesenchymal transition (EMT) scores were generated using KS and 76 GS scores [27,28], and single-sample Gene Set Enrichment Analysis (ssGSEA). PD-L1 activity scores were also obtained using ssGSEA. The KS score uses a two-sample Kolmogorov–Smirnov (KS) test to quantify the E/M (Epithelial/Mesenchymal) status of a given sample. This scoring metric employs 218 gene and 315 gene signatures for tumor and cell line samples, respectively (Table S10). We obtained cumulative distribution functions (CDFs) for the two signatures (Epithelial and Mesenchymal). The maximum distance between these CDFs was utilized as the test statistic for a two-sample KS test giving a final E/M score in the range of $[-1, 1]$. Positive and negative scores denote mesenchymal and epithelial phenotypes, respectively. The 76 GS method utilizes 76 gene signatures to calculate E/M scores for each sample (Table S10). The score of each sample is subtracted from the mean of all samples such that the resulting mean score is zero. The negative scores indicate a mesenchymal phenotype, whereas positive scores represent an epithelial phenotype. The 76 GS score does not have a defined range.

2.3. Single-sample Gene Set Enrichment Analysis

Single-sample Gene Set Enrichment Analysis (ssGSEA) assigns an enrichment score for each sample pairing with a given gene set which signifies the degree of enrichment of that set of genes from a given pathway toward the top or bottom of an input list. It utilizes a pre-processed sample-wise gene expression matrix as input and generates scores using a distinct algorithm [29]. To obtain ssGSEA scores for different pathways, we obtained hallmark genesets (as described below) from the MSigDB repository and calculated the scores for each sample using the GSEAPY python library.

2.4. Genesets used for analysis

Genesets for hallmark EMT, FAO, OXPHOS, glycolysis, HIF-1α and PD-L1 were obtained from MSigDB. Genes used to obtain KS scores previously, were used as genesets for calculating the KS epithelial and mesenchymal scores separately (referred as 'Epi' and 'Mes' scores) (Table S10). ssGSEA scores were calculated using the GSEAPY python library for all datasets with genesets to obtain normalized enrichment scores (NES) for each pathway across all samples.

2.5. Status of oncovirus infection

Each sample was assigned oncovirus-positive or oncovirus-negative status based on the infection status reported by the authors of that dataset available on NCBI-GEO. The number of oncovirus-positive and oncovirus-negative samples in each dataset has been included in Table S9.

2.6. Correlation analysis

Correlation between scores obtained from different EMT scoring metrics and between EMT scores and ssGSEA scores for metabolism and PD-L1 were calculated using Pearson's correlation. A two-tailed Student's t-test with unequal variance was performed to determine the statistical reliability of the observations ($p < 0.05$). Only those datasets were considered whose correlation coefficient (R) was less than -0.3 (significant negative correlation) or greater than 0.3 (significant positive correlation). Similar parameters were set as the cut-off for the 2D

correlation plots. Comparison between metrics and generation of plots and figures was carried out using R (version 4.1.2).

2.7. Comparison between oncovirus positive and negative samples

To check if oncovirus-positive samples were enriched in a pathway, the mean score of enrichment of each pathway in oncovirus-positive samples was compared with that of oncovirus-negative samples for each dataset. Datasets showing a significant difference between the means are analyzed *($p < 0.05$)*.

2.8. Probability plots

For quantifying the probability of a dataset correlating significantly ($p < 0.05$), either positively ($r > 0.3$) or negatively ($r < -0.3$) for a given pair of metrics in the expected direction of the association, the probability was calculated as the ratio of the number of datasets showing a significant correlation in the expected direction (positive correlation for Mes vs. KS and Epi vs. 76 GS, negative correlation for Mes vs. 76 GS and Epi vs. KS) to the total number of datasets showing a significant correlation between those two metrics in either direction. The higher this probability value, the better the compliance between the two corresponding EMT scoring metrics.

2.9. Venn diagrams

To assess the degree of overlaps/consistency between each pairwise comparison of EMT scoring metrics as well as between pairs of EMT and metabolic scores applied to our set of 80 datasets, four-way Venn diagrams were plotted. Each of the four sets in the Venn diagrams have a total number equal to the datasets showing a correlation between any two concerned comparisons in the expected direction.

3. Results

3.1. Oncovirus-positive samples associate with a partial EMT phenotype

To quantify the extent of EMT, we used four distinct transcriptomics-based EMT scoring metrics. Two of those metrics are KS [30] and 76 GS [31] scores. Both these metrics use distinct sets of gene lists corresponding to epithelial and mesenchymal phenotypes and generate a score to identify the position of samples along the epithelial-hybrid-mesenchymal spectrum [27,28]. EMT is a non-linear process where cells can take multiple trajectories in the high-dimensional gene expression space, and the loss of epithelial and gain of mesenchymal traits need not always be completely coupled, as is often tacitly assumed [32]. Given these features of EMT, we also quantified the enrichment of epithelial (Epi) and mesenchymal (Mes) signatures separately using single-sample Gene Set Enrichment Analysis (ssGSEA) scores for KS epithelial and KS mesenchymal gene lists, respectively.

A higher KS or Mes score signifies a more mesenchymal phenotype, whereas a higher 76 GS or Epi score signifies a more epithelial state. Thus, as expected, out of the 80 datasets used in this meta-analysis, 53 (66.25%) datasets showed a strong positive correlation between Epi and 76 GS scores (Fig. 1A, Table S1), and 57 (71.25%) datasets displayed a positive association between Mes and KS scores (Fig. 1B). Consistent with these results, KS and Epi scores were significantly negatively correlated with one another in 43 (53.7%) datasets and positively correlated in only 4 (5%) datasets (Fig. 1C). Similarly, KS and 76 GS scores were negatively correlated with one another in 41 (51.2%) datasets and positively correlated in just 6 (7.5%) datasets (Fig. 1D).

Further, the Mes scores predominantly correlated negatively with both the Epi and 76 GS scores (Figs. S1A–B). Among all the above-mentioned six pairwise comparisons,Mes and KS scores had the

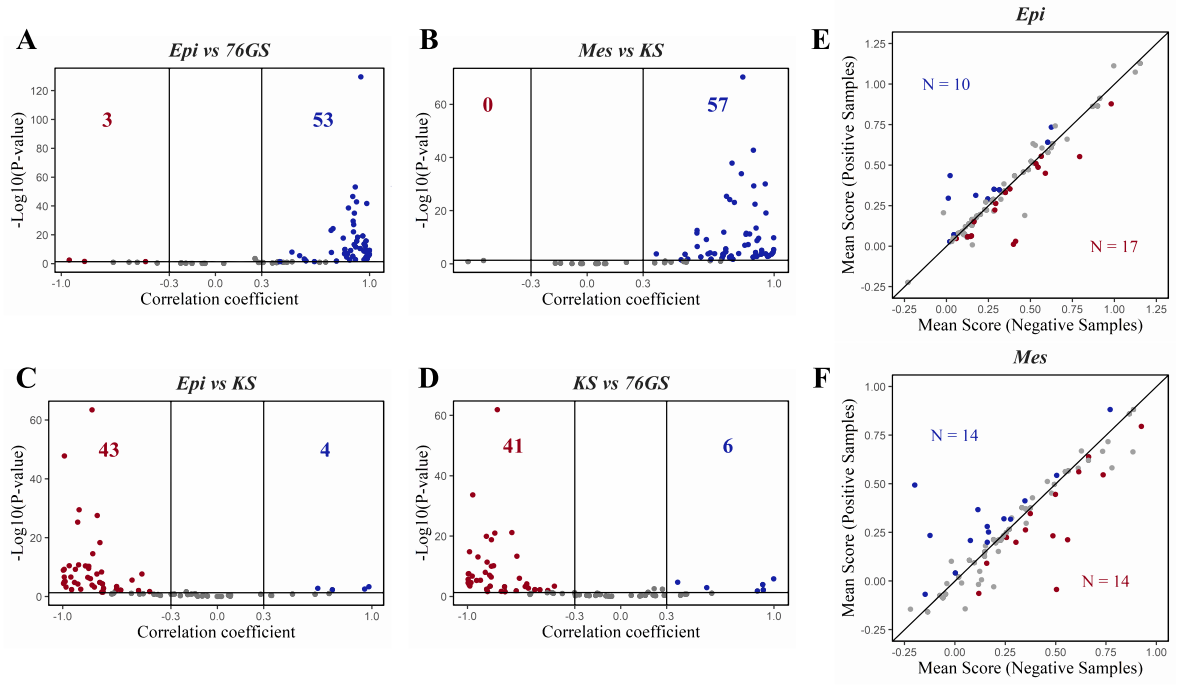

Fig. 1. Different scoring metrics quantify E/M phenotypes in datasets containing oncovirus-infected samples. A) Volcano plot illustrating the Pearson correlation coefficient (x-axis) and the −log10(p-value) (y-axis) for Epi vs. 76 GS scores. Vertical boundaries are set at correlation coefficients corresponding to 0.3 and −0.3 and the cut-off for significant correlation is set at $p < 0.05$. Same as A) but for **B)** Mes vs. KS scores, **C)** Epi vs. KS and **D)** KS vs. 76 GS scores. **E)** Scatter plot depicting mean Epi scores for oncovirus-positive (y-axis) and oncovirus-negative samples (x-axis) across datasets. 'N' indicates the number of datasets with a significant difference between the two mean scores ($p < 0.05$). The datasets with higher mean scores for positive samples are displayed as blue datapoints, while the datasets with higher mean scores for negative samples are shown in red. Datasets with no significant difference in scores for positive vs. negative samples are shown in gray. **F)** Same as E) but for Mes scores. (For interpretation of the references to colour in this figure legend, the reader is referred to the Web version of this article.)

maximum probability of being associated in the expected direction of association, followed by the pairwise association between Epi and 76GS (Fig. S1C). Moreover, the four-way Venn diagram revealed that 31 datasets showed complete consistency among all four pairwise comparisons, i.e., KS scores are negatively correlated with Epi scores but positively with Mes scores, and 76 GS scores are positively correlated with Epi scores but negatively with Mes scores (Fig. S1D). Collectively, these observations highlight the consistency between these scoring metrics in analyzing EMT-related changes in these datasets containing oncovirus-positive and oncovirus-negative samples.

Next, using these metrics, we investigated whether there was a difference in the epithelial and/or mesenchymal status of the oncovirus-positive vs. that of oncovirus-negative samples. For each dataset, we calculated the mean Epi score and the mean Mes score for all oncovirus-positive and oncovirus-negative samples. In 27 out of 80 datasets, we noticed a significant ($p < 0.05$) difference in the mean Epi scores between oncovirus-positive and oncovirus-negative samples. In 17 out of those 27 datasets (63%), oncovirus-negative samples had a higher Epi score than oncovirus-positive samples, suggesting that the epithelial gene signature can be downregulated in the presence of an oncovirus infection (Fig. 1E, Table S8). For the Mes geneset, 28 datasets showed a significant difference *($p < 0.05$)* in the mean scores, and in 14 of those datasets (50%), oncovirus-positive samples showed a higher Mes score than the oncovirus-negative ones, while in the remaining 14 (50%) datasets, an opposite trend was observed (Fig. 1F). Thus, this analysis suggests that the oncovirus-positive samples do not have an enriched mesenchymal status as compared to oncovirus-negative samples. Among the 14 datasets where the Mes scores were higher for oncovirus-positive samples as compared to oncovirus-negative ones, 6 datasets had higher Epi scores while 5 datasets had lower Epi scores for oncovirus-positive samples (Fig. S2B). Similarly, among the 10 datasets where the Epi scores were higher for oncovirus-positive samples as compared to oncovins-negative ones, 5 datasets had higher Mes scores while 3 had lower Mes scores for the oncovirus-positive ones (Fig. S2A). These trends suggest that suppression of epithelial and induction of mesenchymal programs do not always happen simultaneously, thus enabling a partial EMT or hybrid E/M phenotype of oncovirus-positive samples.

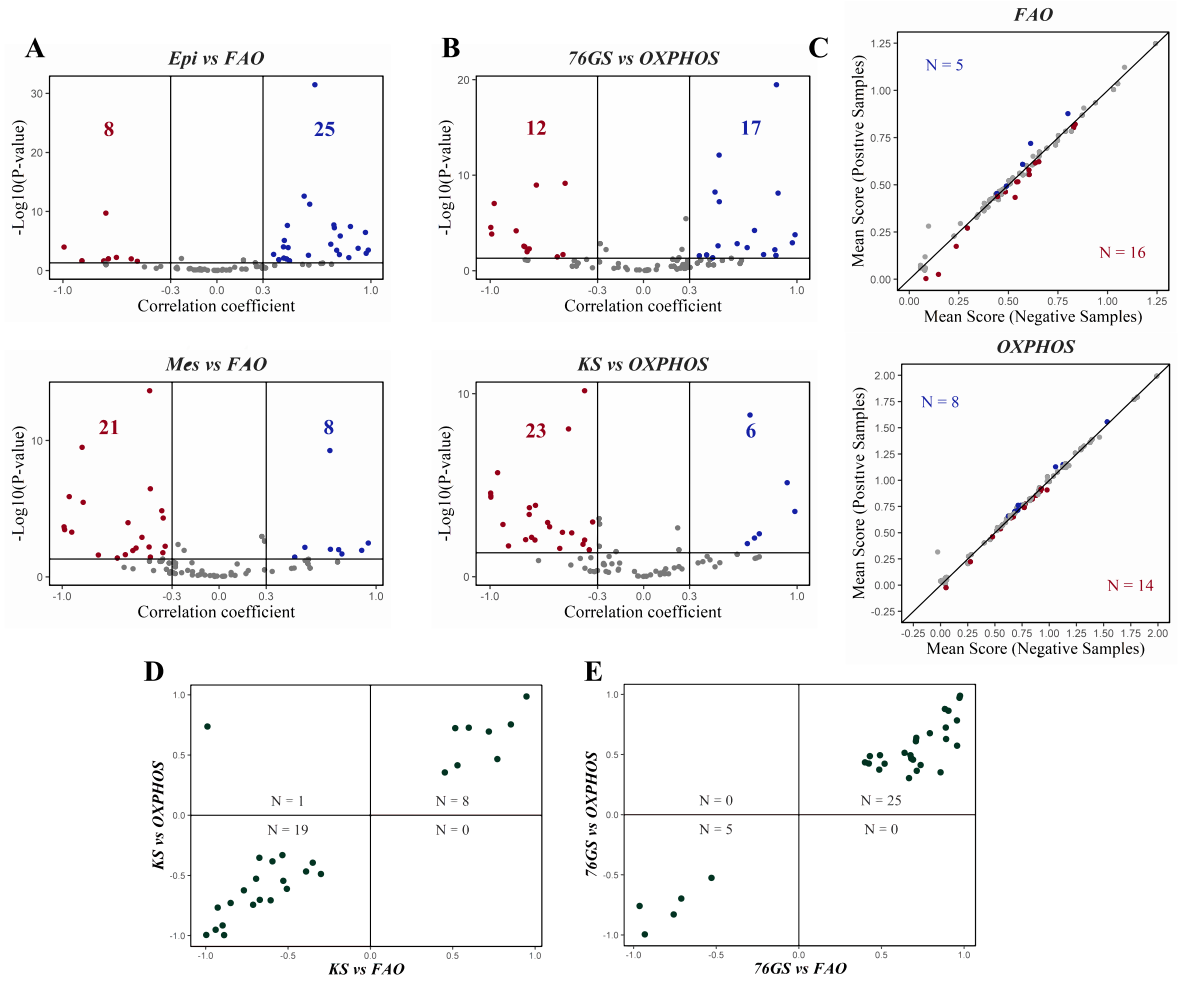

Fig. 2. Association of EMT with OXPHOS and FAO programs in oncovirus-positive samples. A) Volcano plot illustrating the Pearson correlation coefficient (x-axis) and the −log10(p-value) (y-axis) for Epi vs. FAO scores (top) and Mes vs. FAO scores (bottom). Vertical boundaries are set at correlation coefficients corresponding to 0.3 and −0.3, and the cut-off for significant correlation is set at $p < 0.05$. **B)** Same as A) but for 76 GS vs. OXPHOS scores (top) and KS vs. OXPHOS scores (bottom). **C)** Scatter plots depicting mean FAO (top) and OXPHOS scores (bottom) for oncovirus-positive (y-axis) and negative samples (x-axis) across datasets. 'N' indicates the number of datasets with a significant difference between the two mean scores ($p < 0.05$). The datasets with higher mean scores for positive samples are displayed as blue datapoints, while the datasets with higher mean scores for negative samples are shown in red. The datasets showing no significant difference ($p > 0.05$) in mean scores for positive and negative samples are shown in gray. **D)** 2D scatter plot illustrating correlation coefficients of KS vs. FAO scores (x-axis) and KS vs. OXPHOS (y-axis). 'N' indicates the number of datasets that lie in the respective quadrant. **E)** Same as D) but for 76 GS vs. FAO scores (x-axis) and 76 GS vs. OXPHOS (y-axis). (For interpretation of the references to colour in this figure legend, the reader is referred to the Web version of this article.)

3.2. Oncovirus-positive samples have reduced OXPHOS and FAO activity levels

Our previous pan-cancer meta-analysis for 180 datasets revealed that EMT was associated with a decreased activity of oxidative phosphorylation (OXPHOS) and fatty acid oxidation (FAO) pathways [15]. We capitalized on this analysis to dissect differences in OXPHOS and FAO levels for oncovirus-positive vs. oncovirus-negative samples. To do this, we first probed whether the earlier observed association between EMT and metabolic reprogramming was found in oncovirus-infected samples and quantified differences in metabolic activity of the oncovirus-positive vs. oncovirus-negative samples.

First, we correlated the ssGSEA scores of hallmark metabolic pathways–fatty acid oxidation (FAO) and oxidative phosphorylation (OXPHOS) with EMT scoring metrics across datasets. FAO predominantly correlated positively with an epithelial gene signature and negatively with a mesenchymal gene signature. A total of 25 out of 80 datasets had positive correlations between FAO and Epi scores, with eight datasets showing an opposite trend. Similarly, FAO and Mes scores correlated negatively in 21 datasets and displayed the reverse trend in only eight datasets (Fig. 2A, Table S2). Consistent results were observed when correlating FAO enrichment with the 76 GS and KS scores (Fig. S3A). Together, these results are reminiscent of our previous observations [15] and consistent with reports that virus infection leads to a shift from fatty acid oxidation to fatty acid synthesis [33].

Similar to the trends observed for FAO, OXPHOS also correlated positively with an epithelial state in most data sets. Upon correlating OXPHOS with EMT scores, we found that OXPHOS primarily correlated negatively with a mesenchymal program and positively with an epithelial program – 23 datasets displayed a negative correlation between OXPHOS and KS scores, in comparison only six datasets showed the reverse trend (Fig. 2B, bottom: Table S3). Similar behavior was evident when using Mes scores (Fig. S3B). On the other hand, the relationship between OXPHOS and epithelial scores was more ambiguous. While 17 datasets showed a positive correlation of OXPHOS with 76 GS, 12 displayed a negative correlation. Similarly, in 14 datasets, OXPHOS correlated positively with an Epi score, but in 15 datasets, an opposite trend was observed (Fig. 2B, top; Fig. S3B). Together, these analyses suggest that OXPHOS is more likely to correlate negatively with a mesenchymal phenotype (i.e., KS and Mes scores) in the context of oncovirus-infected samples.

Next, we quantified the mean OXPHOS and FAO scores to interrogate changes in metabolic reprogramming in oncovirus-positive and oncovirus-negative samples. A total of 21 out of 80 datasets showed a significant ($p < 0.05$) difference in mean FAO scores for oncovirus-positive and oncovirus-negative samples. Only 5 out of 21 datasets (23.8%) had a higher FAO score for oncovirus-positive samples compared to oncovirus-negative ones, while in 16 datasets (76.2%), oncovirus-negative samples had a higher FAO pathway enrichment score. Similar results were found in the case of OXPHOS, wherein 14 out of 22 datasets (63.6%) had a higher OXPHOS score for oncovirus-negative samples (Fig. 2C). These analyses suggest that both FAO and OXPHOS are often downregulated in oncovirus-positive samples.

We also examined the pairwise associations between OXPHOS and FAO to interrogate if some combinations of association were more predominant than others in the context of their correlation with EMT. For instance, in 28 datasets, KS scores were significantly correlated with both FAO and OXPHOS scores, either positively or negatively. Among these 28 datasets, in 19 datasets (67.9%), the KS scores correlated negatively with both FAO and OXPHOS; in 8 datasets (29.6%), FAO and OXPHOS both correlated positively with KS scores (Fig. 2D). Similar trends were observed when using other EMT scoring metrics – 76 GS (Fig. 2E), Epi and Mes (Fig. S3C). FAO and OXPHOS scores correlated either positively or negatively with 76 GS scores in 30 datasets. In 25 out of the 30 datasets (83.3%), 76 GS scores correlated positively with both FAO and OXPHOS, while in 5 datasets (16.7%), they correlated negatively (Fig. 2E). Also, among the 10 datasets in which Epi scores were higher for oncovirus-positive samples, 7 datasets had lower OXPHOS scores for oncovirus-positive samples (Fig. S5). Together, these results suggest that oncovirus-positive samples tend to have reduced OXPHOS and FAO activity, a pattern consistent with their partial EMT state and with our previous pan-cancer observations linking partial EMT with alterations in metabolism [15]. Interestingly, the association between EMT and FAO is stronger than that for EMT with OXPHOS in the context of oncovirus infection.

3.3. Oncovirus-positive samples exhibit enrichment of glycolysis

After investigating the changes in OXPHOS and FAO levels, we tested for changes in glycolysis levels. Glycolysis is often upregulated in cancer cells (Warburg effect) to compensate for an increased ATP demand, proliferation, and survival [34]. To analyze the association of glycolysis with the process of EMT, we calculated ssGSEA enrichment scores for the hallmark glycolysis gene set and correlated the ssGSEA scores with different EMT scoring metrics across the 80 datasets.

We observed that glycolysis correlated positively with both epithelial and mesenchymal signatures (Fig. 3A, S4A, Table S4). This trend seems unexpected according to the canonical EMT paradigm in which epithelial and mesenchymal programs are thought to be strongly antagonistic to one another and expected to associate with diverse phenomena in opposite directions. However, EMT is a multi-dimensional process in which downregulation of an epithelial program is not necessarily strongly connected to the upregulation of a mesenchymal program and *vice versa*, thereby allowing multiple trajectories in terms of molecular and functional changes [35]. From this perspective, it is perhaps not surprising that a positive association exists between glycolysis and both epithelial and mesenchymal programs (Fig. 3A, top: 31 out of 36 datasets show a positive correlation with epithelial; Fig. 3A, bottom: 23 out of 29 datasets show positive correlation with mesenchymal). To further interrogate these relationships, we analyzed the relationship between epithelial and mesenchymal scores with HIF-1α, a known mediator of the glycolytic pathway. Consistent with the relationships between glycolysis and EMT scores, the HIF-1α pathway correlated positively with both an epithelial and a mesenchymal program. In 23 out of 29 datasets (79.3%), HIF-1α correlated positively with the epithelial signature while it correlated positively with the mesenchymal signature in 28 out of 30 datasets (93.3%) (Fig. 3B, Table S5). Similar relationships existed between HIF-1α and 76 GS and KS scores (Fig. S4B). In 16 out of 27 (59.3%) datasets, glycolysis activity levels showed a higher score for oncovirus-positive samples as compared to oncovirus-negative samples. For HIF-1α activity levels, 66.6% of datasets (18 out of 27) had a higher HIF1α activity score for oncovirus-positive samples (Fig. 3C). These trends point towards glycolysis upregulation in the presence of an oncovirus infection.

We next asked whether the glycolysis pathway gene set correlated positively with epithelial and mesenchymal programs in the same datasets. Pairwise correlations between glycolysis and epithelial and mesenchymal gene signatures indicated that glycolysis correlates positively with both Epi and Mes scores (17/26 = 65.4% datasets) (Fig. 3D). A similar association was observed in the case of HIF-1α, with HIF-1α correlating positively with both the epithelial and mesenchymal programs in 16 out of 23 datasets (69.6%) (Fig. 3E). Similarly, glycolysis scores were also significantly higher in 50% datasets with higher Epi scores for oncovirus-positive samples while 36% had an enriched glycolysis signature in datasets with high Mes scores for positive vs. negative samples (Fig. S5).

Overall, the positive association of glycolysis and its major driver, HIF-1α, with both epithelial and mesenchymal gene signatures suggests that glycolysis may be correlated with a partial EMT program. This association may underlie the observations about enrichment of glycolysis in oncovirus-positive samples (Fig. 3C), given the enrichment of partial EMT status in these samples (Fig. 1E–F).

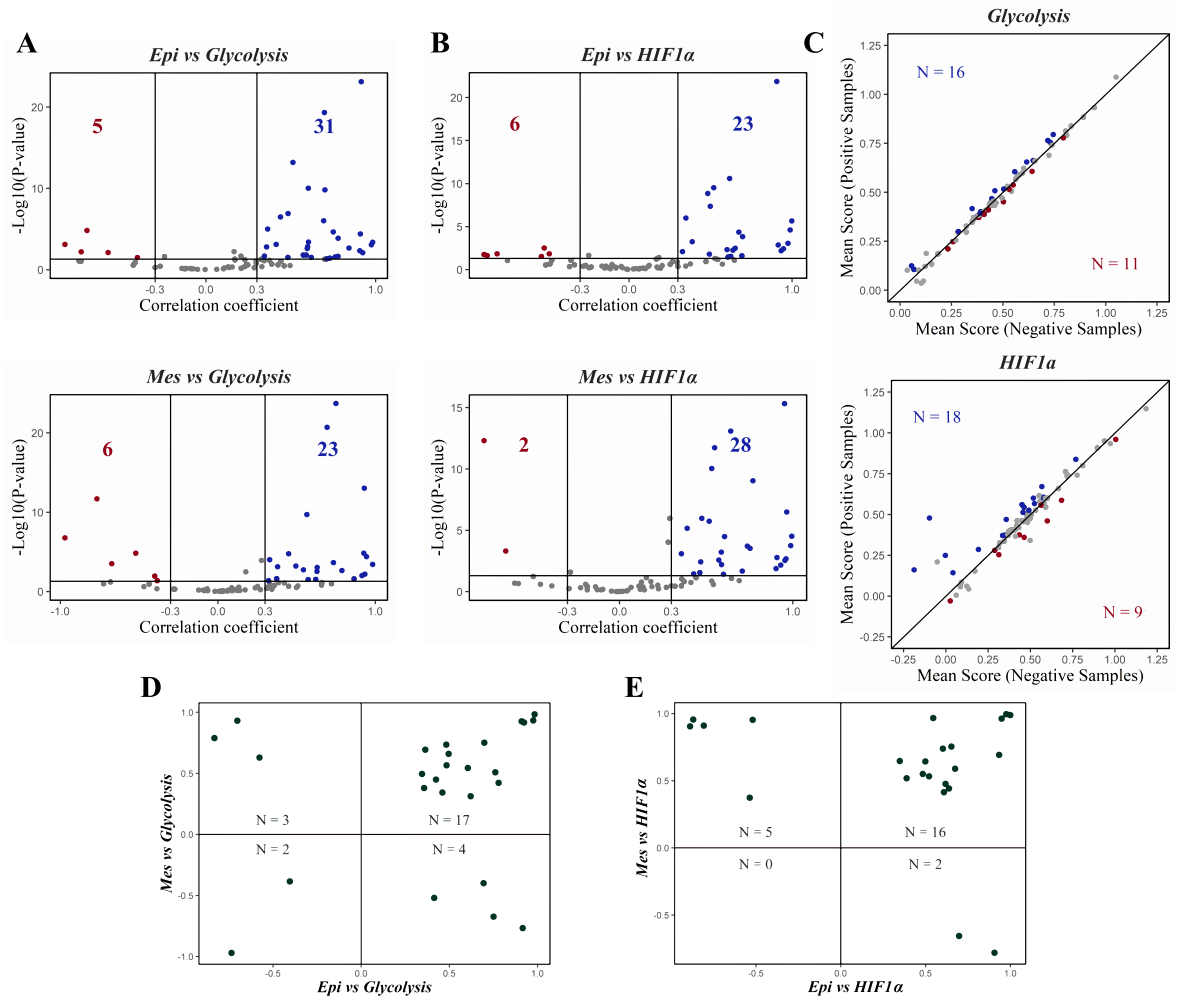

Fig. 3. Association of glycolysis activity level (and its master regulator HIF-1α) with partial EMT and oncovirus infection. A) Volcano plot illustrating the Pearson correlation coefficient (x-axis) and the −log10(p-value) (y-axis) for Epi vs. Glycolysis scores (top) and Mes vs. Glycolysis scores (bottom). Vertical boundaries are set at correlation coefficients corresponding to 0.3 and −0.3, and the cut-off for significant correlation is set at $p < 0.05$. **B)** Same as A) but for Epi vs. HIF1α (top) and Mes vs. HIF1α scores (bottom). **C)** Scatter plots depicting mean FAO (top) and OXPHOS scores (bottom) for oncovirus-positive (y-axis) and negative samples (x-axis) across datasets. 'N' indicates the number of datasets with a significant difference between the two mean scores ($p < 0.05$). The datasets with higher mean scores for positive samples are displayed as blue datapoints, while the datasets with higher mean scores for negative samples are shown in red. The datasets showing no significant difference ($p > 0.05$) in mean scores for positive and negative samples are shown in gray. **D)** 2D scatter plot illustrating correlation coefficients of Epi vs. Glycolysis scores (x-axis) and Mes vs. Glycolysis (y-axis). 'N' indicates the number of datasets that lie in the respective quadrant. **E)** Same as D) but for Epi vs. HIF1α scores (x-axis) and Mes vs. HIF1α (y-axis). (For interpretation of the references to colour in this figure legend, the reader is referred to the Web version of this article.)

3.4. Enrichment of PD-L1 signature in oncovirus-positive samples and associated changes in EMT and metabolic reprogramming

Oncoviruses such as EBV and HPV have been associated with increased PD-L1 levels [25]. Likewise, EMT is also correlated with the upregulation of immune checkpoints [36,37]. These relationships prompted us to investigate whether oncovirus-positive samples were enriched in PD-L1 activity and/or expression. Out of 26 datasets that showed a difference in mean PD-L1 activity levels for oncovirus-positive vs. oncovirus-negative samples, 18 (69.2%) datasets showed a higher PD-L1 activity score for oncovirus-positive samples as compared to oncovirus-negative samples (Fig. 4A, top). Similar trends were noticed for expression levels of *CD274* (gene encoding for PD-L1) (Fig. 4A, bottom). A total of 12/21 (57.1%) datasets displayed significant *($p < 0.05$)* upregulation of *CD2 74* mRNA levels for oncovirus-positive samples as compared to oncovirus-negative samples. Overall, this enrichment of the PD-L1 pathway signature in oncovirus-positive samples suggests a possible relationship between oncovirus infection and upregulation of immune checkpoints like PD-L1 and its associated gene, *CD274*.

After examining the association of oncovirus infection in samples with enrichment of the PD-L1 pathway gene set across datasets, we investigated the trends between changes in levels of Epi, Mes scores, and activity of the PD-L1 geneset simultaneously. Here, we discuss four representative datasets, one each for a different oncovirus, and we noticed that PD-L1 activity and Mes scores increase in all cases to varying degrees when comparing oncovirus-positive and oncovirus-negative samples. Similarly, except for HCV, Epi scores are lower for oncovirus-positive samples as compared to oncovirus-negative samples (Fig. 4B). Together, these observations suggest that the changes in Epi, Mes, and PD-L1 activity scores can be coordinated and thus observed concomitantly.

Given the relationship between PD-L1 and EMT [36,37], we also analyzed the correlations between PD-L1 activity and EMT scores across our entire cohort of datasets. We observed that the PD-L1 activity was more likely to correlate positively with a Mes score (22 out of 28 datasets in Fig. 4C, Table S6) than with an Epi signature (15 out of 28 datasets in Fig. 4C). Furthermore, a similar trend was observed for *CD274* mRNA

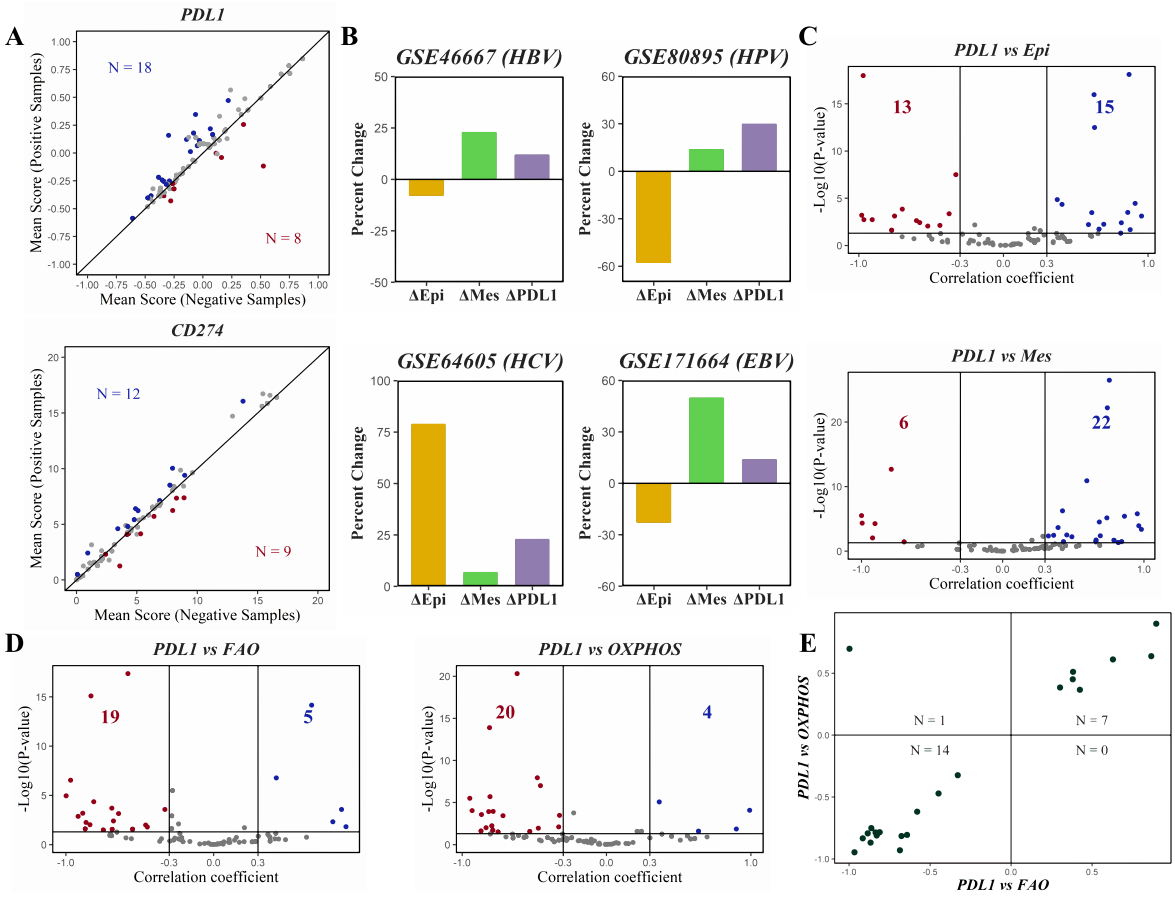

Fig. 4. Oncovirus-induced EMT-related changes in PD-L1 and different metabolic axes. A) Scatter plots depicting mean PD-L1 scores (top) and CD274 gene expression values (bottom) for oncovirus-positive (y-axis) and negative samples (x-axis) across datasets. 'N' indicates the number of datasets with a significant difference between the two mean scores ($p < 0.05$). The datasets with higher mean scores for positive samples are displayed as blue datapoints, while the datasets with higher mean scores for negative samples are shown in red. The datasets showing no significant difference ($p > 0.05$) in mean scores for positive and negative samples are shown in gray. **B)** Bar plots depicting relative percentage change (of positive samples with respect to negative samples) in Epi (yellow), Mes (green), and PD-L1 (purple) scores for particular datasets (denoted by GSE IDs). **C)** Volcano plots illustrating the Pearson correlation coefficient (x-axis) and the −log10(p-value) (y-axis) for PD-L1 vs. Epi score (top) and PD-L1 vs. Mes score (bottom). Vertical boundaries are set at correlation coefficients corresponding to 0.3 and −0.3, and the cut-off for significant correlation is set at $p < 0.05$. **D)** Same as C) but for PD-L1 vs. FAO scores (left), and PD-L1 vs. OXPHOS scores (right). **E)** 2D scatter plot illustrating correlation coefficients of PD-L1 vs. FAO (x-axis) and PD-L1 vs. OXPHOS scores (y-axis). 'N' indicates the number of datasets that lie in the respective quadrant. (For interpretation of the references to colour in this figure legend, the reader is referred to the Web version of this article.)

levels versus Epi and Mes scores (Figs. S6D–E). These analyses suggest that enrichment of PD-L1 scores is more aligned with the presence of a mesenchymal signature rather than the absence of an epithelial one. This trend also highlights a potential association of PD-L1 with a partial EMT program, as noted experimentally [14,38,39] in which a loss of epithelial traits and gain of mesenchymal ones can be considered as semi-independent properties [35]. Moreover, upon plotting the pairwise association of PD-L1 with FAO and OXPHOS, the predominant association observed was that a PD-L1 signature correlated negatively with both pathways, as observed in 63.6% of datasets (Fig. 4D–E). Interestingly, PD-L1 activity was also correlated negatively with glycolysis (Fig. S6A). Overall, these analyses suggest that the PD-L1 activity signature is likely to be negatively associated with metabolic reprogramming in oncovirus-infected samples.

3.5. Oncovirus infection is associated with the upregulation of immune checkpoint markers

We also determined the association between the presence of oncovirus infection and mRNA expression levels of additional immune checkpoint markers, including *CD276* (encodes B7-H3), *CD47* (encodes Cluster of Differentiation 47), *HAVCR2* (encodes TIM-3) and *LGALS9* (encodes galectin 9) [40–42]. Similar to trends seen for *CD274*, oncovirus-positive samples showed a significant upregulation in mRNA levels of *CD47* (78.2% of datasets), *HAVCR2* (64.7%), and *LGALS9* (71.4%) as compared to oncovirus-negative ones (Fig. 5A). However, *CD276* did not show any such enrichment.

Correlation of transcript levels of these genes with epithelial and mesenchymal signatures revealed that *CD276* and *CD47* correlated positively with both Epi and Mes scores, although the association was stronger with the mesenchymal score than the epithelial score (Fig. 5B, S7A, B, Table S7). Expression of *HAVCR2* showed a positive correlation with the Mes score (16 vs. 6 as in Fig. 5B) but negatively with the Epi score (14 vs. 7 as in Fig. S7C). An antagonistic trend was seen with *LGALS9* which correlated primarily positively with epithelial signature (19 vs. 4) but negatively with mesenchymal one (11 vs. 9) (Figs. 7D and 5B). Thus, similar to PD-L1, additional immune checkpoint markers also seem to associate with a partial EMT signature.

Next, we compared the pairwise association of these four immune checkpoint markers with epithelial and mesenchymal scores. The predominant trend observed for all the genes was that the expression levels correlated positively with both epithelial and mesenchymal programs, with some checkpoints (except LGALS9) correlating positively with the mesenchymal program and negatively with epithelial scores. However,

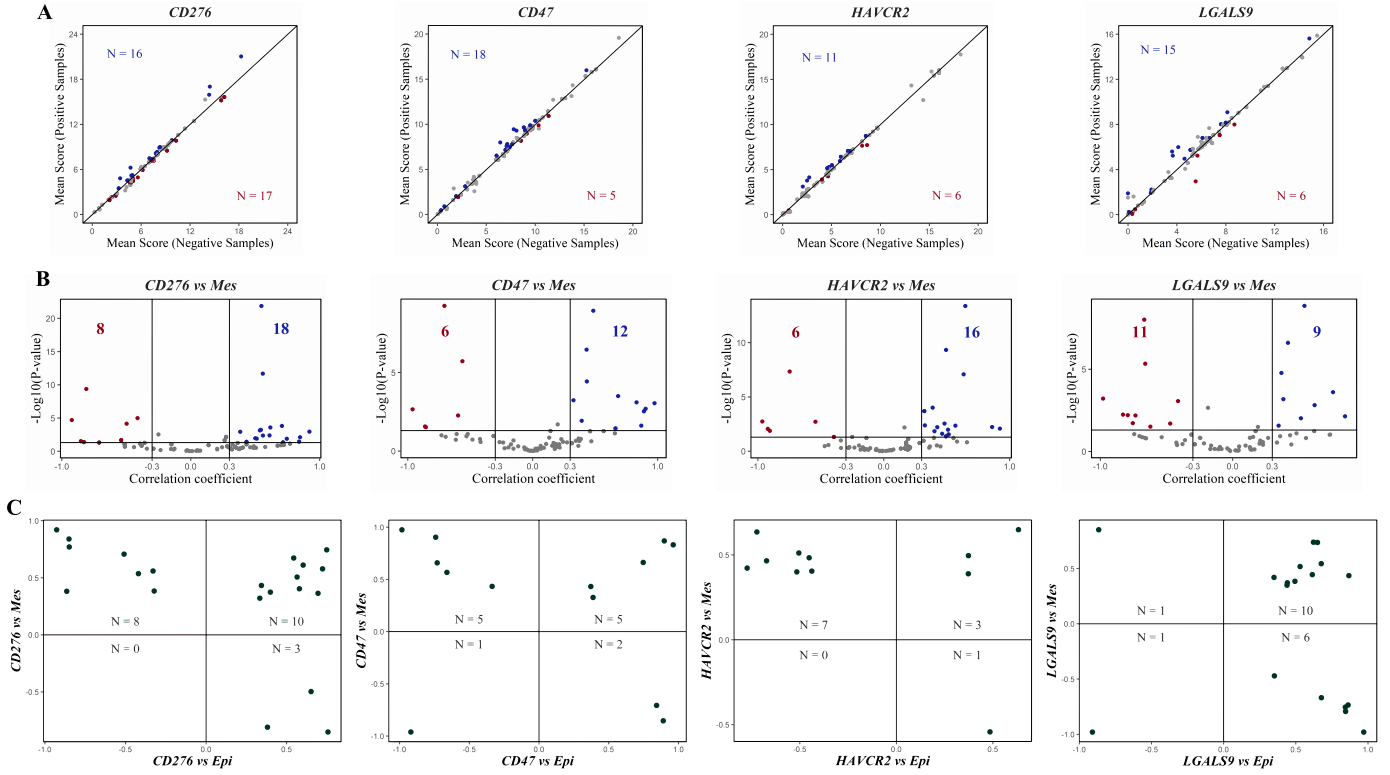

Fig. 5. Association of gene expression of different immune checkpoints with EMT and oncovirus infection. A) Scatter plots depicting the mean expression values for oncovirus-positive (y-axis) and negative samples (x-axis) across datasets: (from left to right) *CD276*, *CD47*, *HAVCR2* and *LGALS9*. 'N' indicates the number of datasets with a significant difference between the two mean scores ($p < 0.05$). Datasets with higher mean scores for positive samples are displayed as blue datapoints, while those with a higher mean scores for negative samples are shown in red. Datasets showing no significant difference ($p > 0.05$) in mean scores for positive and negative samples are shown in gray. **B)** Volcano plots illustrating the Pearson correlation coefficient (x-axis) and the $-\log_{10}$(p-value) (y-axis) for*CD276* vs. Mes (left), *CD47* vs. Mes (middle-left), *HAVCR2* vs. Mes (middle-right) and *LGALS9* vs. Mes scores (right). Vertical boundaries are set at correlation coefficients corresponding to 0.3 and −0.3, and $p < 0.05$. **C)** 2D scatter plot illustrating correlation coefficients of *CD276* vs. Epi scores (x-axis) & *CD276*vs. Mes (y-axis) (left), *CD47* vs. Epi scores (x-axis) & *CD47* vs. Mes (y-axis) (middle-left), *HAVCR2* vs. Epi scores (x-axis) & *HAVCR2* vs. Mes (y-axis) (middle-right) and HAVCR2 vs. Epi scores (x-axis) & *HAVCR2* vs. Mes (y-axis) (right). 'N' indicates the number of datasets that lie in the respective quadrant. (For interpretation of the references to colour in this figure legend, the reader is referred to the Web version of this article.)

for *LGALS9*, the opposite trend was observed i.e., *LGALS9* gene expression correlated negatively with epithelial scores but positively with mesenchymal ones (Fig. 5C), supporting an association between partial or full EMT and upregulation of these immune checkpoints in oncovirus-positive samples.

4. Discussion

Oncoviruses have been associated with multiple cancer hallmarks [43], including metastasis and chemoresistance, and the formation of polyploid giant cancer cells [44,45]. Detailed molecular investigations into the oncovirus-driven alterations in cellular behavior can be instrumental in decoding how oncoviruses impact multiple stages of cancer progression and may pinpoint novel therapeutic strategies [46].

Here, we performed a meta-analysis of oncovirus-positive samples in interconnected axes of cellular plasticity: EMT, metabolic reprogramming, and immune checkpoint expression [14,39,47–49]. While crosstalk among these axes has been investigated in multiple cancers, their interconnection, specifically in oncovirus-positive scenarios, remains poorly understood. Our analyses identified consistent correlations between EMT, metabolism and PD-L1 levels across oncoviruses using bulk transcriptomics data. In particular, these analyses revealed that FAO and OXPHOS pathway activity is often decreased in samples with a strong enrichment of EMT signatures, implying a common adaptative mechanism connecting EMT and metabolic reprogramming. Despite identifying this consistent relationship, we were not able to pinpoint specific molecules mediating this interconnection or dissect how EMT and FAO (or OXPHOS) may influence one another. Intriguingly, glycolysis was higher in samples expressing both epithelial and mesenchymal genes, suggesting that glycolysis is likely to be associated with a hybrid E/M phenotype. This observation is reminiscent of the increase in glycolysis observed upon treatment with TGFβ, a canonical EMT inducer [50]. Given that most studies focus on bulk-level analysis at limited time-points, it is challenging to convincingly demonstrate an association between hybrid E/M phenotype(s) and glycolysis; however, developing novel lineage tracing/barcoding strategies, coupled with single-cell metabolomics, may pave the way for further investigation into the dynamics of cellular plasticity at different spatiotemporal coordinates in cancer evolution [51].

We also observed scenarios where immune checkpoints, such as PD-L1, correlated negatively with both OXPHOS and glycolysis, indicating that these axes of metabolic reprogramming are not strictly antagonistic. These indications are strengthened by observations of high glycolysis/high OXPHOS and low glycolysis/low OXPHOS phenotypes, in addition to canonical high glycolysis/low OXPHOS and low glycolysis/high OXPHOS ones [52–54]. However, in contrast to our analyses, glycolysis has been reported to enhance PD-L1 levels in cancer cells [55]. Further investigations shall be needed to better understand the context-specific mechanistic underpinnings and between immune evasion and metabolic plasticity. Another angle to investigate further in oncovirus-positive samples is stemness, given its association with metabolic reprogramming and EMT in many cancers [56,57]. Overall, our results show consistent trends in terms of EMT, metabolic plasticity, and immune checkpoint expression in oncovirus-positive samples.

Funding

This research was supported by Ramanujan Fellowship (SB/S2/RJN-049/2018) awarded to MKJ by Science & Engineering Research Board (SERB), Department of Science & Technology, Government of India.

Author contributions

MKJ designed research; MKJ and JAS supervised research; MS, RR, JMV & SK performed research and analyzed the data; MS and RR prepared a first draft of the manuscript, which all co-authors revised.

Declaration of competing interest

The authors declare that they have no known competing financial interests or personal relationships that could have appeared to influence the work reported in this paper.

Data availability

The data used is publicly available, and the GEO dataset IDs are provided.

Appendix A. Supplementary data

Supplementary data to this article can be found online at https://doi.org/10.1016/j.adcanc.2023.100091.

References

[1] M.E. McLaughlin-Drubin, K. Munger, Viruses associated with human cancer, Biochim. Biophys. Acta, Mol. Basis Dis. 1782 (2008) 127–150, https://doi.org/10.1016/j.bbadis.2007.12.005.
[2] J. Cao, D. Li, Searching for human oncoviruses: histories, challenges, and opportunities, J. Cell. Biochem. 119 (2018) 4897–4906, https://doi.org/10.1002/jcb.26717.
[3] W.M. Xiong, Q.P. Xu, X. Li, et al., The association between human papillomavirus infection and lung cancer: a system review and meta-analysis, Oncotarget 8 (2017) 96419–96432, https://doi.org/10.18632/oncotarget.21682.
[4] B. Yin, W. Liu, P. Yu, et al., Association between human papillomavirus and prostate cancer: a meta-analysis, Oncol. Lett. 14 (2017) 1855–1865, https://doi.org/10.3892/ol.2017.6367.
[5] N. Khodabandehlou, S. Mostafaei, A. Etemadi, et al., Human papilloma virus and breast cancer: the role of inflammation and viral expressed proteins, BMC Cancer 19 (2019) 61, https://doi.org/10.1186/s12885-019-5286-0.
[6] H.B. El-Serag, Epidemiology of viral hepatitis and hepatocellular carcinoma, Gasteroenterology 142 (2012) 1254–1273.e1, https://doi.org/10.1052/j.gastro.2011.12.061.
[7] M.L. Tornesello, C. Annunziata, A.L. Tornesello, et al., Human oncoviruses and p53 tumor suppressor pathway deregulation at the origin of human cancers, Cancers 10 (2018) 213, https://doi.org/10.3390/cancers10070213.
[8] M.A. Nieto, R.Y. Huang, R.A. Jackson, J.P. Thiery, EMT: 2016, Cell 166 (2016) 21–45, https://doi.org/10.1016/j.cell.2016.06.028.
[9] K.M. Hajra, D.Y.-S. Chen, E.R. Fearon, The SLUG zinc-finger protein represses E-cadherin in breast cancer, Cancer Res. 62 (2002) 1613–1618.
[10] J. Yang, S.A. Mani, J.L. Donaher, et al., Twist, a master regulator of morphogenesis, plays an essential role in tumor metastasis, Cell 117 (2004) 927–939, https://doi.org/10.1016/j.cell.2004.06.006.
[11] C. Wels, S. Joshi, P. Koefinger, et al., Transcriptional activation of ZEB1 by slug leads to cooperative regulation of the epithelial–mesenchymal transition-like phenotype in melanoma, J. Invest. Dermatol. 131 (2011) 1877–1885, https://doi.org/10.1038/jid.2011.142.
[12] A. Dongre, M. Rashidian, F. Reinhardt, et al., Epithelial-to-mesenchymal transition contributes to immunosuppression in breast carcinomas, Cancer Res. 77 (2017) 3982–3989, https://doi.org/10.1158/0008-5472.CAN-16-3292.
[13] M. Sciacovelli, C. Frezza, Metabolic reprogramming and epithelial-to-mesenchymal transition in cancer, FEBS J. 284 (2017) 3132–3144, https://doi.org/10.1111/febs.14090.
[14] S. Sahoo, S.P. Nayak, K. Hari, et al., Immunosuppressive traits of the hybrid epithelial/mesenchymal phenotype, Front. Immunol. 12 (2021), 797261, https://doi.org/10.3389/fimmu.2021.797261.
[15] S. Muralidharan, S. Sahoo, A. Saha, et al., Quantifying the patterns of metabolic plasticity and heterogeneity along the epithelial–hybrid–mesenchymal spectrum in cancer, Biomolecules 12 (2022) 297, https://doi.org/10.3390/biom12020297.
[16] S. Kumar, A. Das, S. Sen, Extracellular matrix density promotes EMT by weakening cell-cell adhesions, Mol. Biosyst. 10 (2014) 838–850, https://doi.org/10.1039/c3mb70431a.
[17] X. Li, M.K. Jolly, J.T. George, et al., Computational modeling of the crosstalk between macrophage polarization and tumor cell plasticity in the tumor microenvironment, Front. Oncol. 9 (2019) 10, https://doi.org/10.3389/fonc.2019.00010.
[18] K. Saxena, M.K. Jolly, Acute vs. Chronic vs. cyclic hypoxia: their differential dynamics, molecular mechanisms, and effects on tumor progression, Biomolecules 9 (2019) 339, https://doi.org/10.3390/biom9080339.
[19] C. Gilles, M. Polette, J. Piette, et al., Epithelial-to-mesenchymal transition in hpv-33-transfected cervical keratinocytes is associated with increased invasiveness and expression of gelatinase a, Int. J. Cancer 59 (1994) 661–666, https://doi.org/10.1002/ijc.2910590514.
[20] X. Chen, A.M. Bode, Z. Dong, Y. Cao, The epithelial–mesenchymal transition (EMT) is regulated by oncoviruses in cancer, Faseb. J. 30 (2016) 3001–3010, https://doi.org/10.1096/fj.201600388R.
[21] S. Tripathi, H. Levine, M.K. Jolly, The physics of cellular decision-making during epithelial-mesenchymal transition, Annu. Rev. Biophys. 49 (2020) 1–18, https://doi.org/10.1146/annurev-biophys-121219-081557.
[22] J.G. Purdy, M.A. Luftig, Reprogramming of cellular metabolic pathways by human oncogenic viruses, Curr Opin Virol 39 (2019) 60–69, https://doi.org/10.1016/j.coviro.2019.11.002.
[23] P.J. Mullen, H.R. Christofk, The metabolic relationship between viral infection and cancer, Annu. Rev. Cell Biol. 6 (2022) 1–15, https://doi.org/10.1146/annurev-cancerbio-070120-090423.
[24] P.P. Piccaluga, A. Weber, M.R. Ambrosio, et al., Epstein-barr virus-induced metabolic rearrangements in human B-cell lymphomas, Front. Microbiol. 9 (2018) 1233, https://doi.org/10.3389/fmicb.2018.01233.
[25] H. Farrukh, N. El-Sayes, K. Mossman, Mechanisms of PD-L1 regulation in malignant and virus-infected cells, Int. J. Mol. Sci. 22 (2021) 4893, https://doi.org/10.3390/ijms22094893.
[26] Y. Han, D. Liu, L. Li, PD-1/PD-L1 Pathway: Current Researches in Cancer, Am. J. Cancer Res. 10 (2020) 727–740.
[27] P. Chakraborty, J.T. George, S. Tripathi, et al., Comparative study of transcriptomics-based scoring metrics for the epithelial-hybrid-mesenchymal spectrum, Front. Bioeng. Biotechnol. 8 (2020) 220, https://doi.org/10.3389/fbioe.2020.00220.
[28] S. Mandal, T. Tejaswi, R. Janivara, et al., Transcriptomic-based quantification of the epithelial-hybrid-mesenchymal spectrum across biological contexts, Biomolecules 12 (2022) 29, https://doi.org/10.3390/biom12010029.
[29] S. Aravind, T. Pablo, K. Mv, et al., Gene set enrichment analysis: a knowledge-based approach for interpreting genome-wide expression profiles, Proc. Natl. Acad. Sci. USA 102 (2005) 15545–15550, https://doi.org/10.1073/pnas.0506580102.
[30] T.Z. Tan, Q.H. Miow, Y. Miki, et al., Epithelial-mesenchymal transition spectrum quantification and its efficacy in deciphering survival and drug responses of cancer patients, EMBO Mol. Med. 6 (2014) 1279–1293, https://doi.org/10.15252/emmm.201404208.
[31] L.A. Byers, L. Diao, J. Wang, et al., An epithelial-mesenchymal transition gene signature predicts resistance to EGFR and PI3K inhibitors and identifies Axl as a therapeutic target for overcoming EGFR inhibitor resistance, Clin. Cancer Res. 19 (2013) 279–290, https://doi.org/10.1158/1078-0432.CCR-12-1558.
[32] K. Watanabe, N. Panchy, S. Noguchi, et al., Combinatorial perturbation analysis reveals divergent regulations of mesenchymal genes during epithelial-to-mesenchymal transition, NPJ Syst Biol Appl 5 (2019) 21, https://doi.org/10.1038/s41540-019-0097-0.
[33] D. Sumbria, E. Berber, M. Mathayan, B.T. Rouse, Virus infections and host metabolism—can we manage the interactions? Front. Immunol. 11 (2021), 594963 https://doi.org/10.3389/fimmu.2020.594963.
[34] T. Shiraishi, J.E. Verdone, J. Huang, et al., Glycolysis is the primary bioenergetic pathway for cell motility and cytoskeletal remodeling in human prostate and breast cancer cells, Oncotarget 6 (2015) 130–143, https://doi.org/10.18632/oncotarget.2766.
[35] S. Sahoo, A.S. Duddu, A. Biddle, M.K. Jolly, Interconnected high-dimensional landscapes of epithelial-mesenchymal plasticity and stemness, Clin. Exp. Metastasis 39 (2022) 279–290, https://doi.org/10.1007/s10585-021-10139-2.
[36] K.E. Ware, S. Gupta, J. Eng, et al., Convergent evolution of p38/MAPK activation in hormone resistant prostate cancer mediates pro-survival, immune evasive, and metastatic phenotypes, bioRxiv (2020), https://doi.org/10.1101/2020.04.22.050385, 2020.04.22.050385.
[37] P. Chakraborty, E.L. Chen, I. McMullen, et al., Analysis of immune subtypes across the epithelial-mesenchymal plasticity spectrum, Comput. Struct. Biotechnol. J. 19 (2021) 3842–3851, https://doi.org/10.1016/j.csbj.2021.06.023.
[38] V. Aggarwal, C.A. Montoya, V.S. Donnenberg, S. Sant, Interplay between tumor microenvironment and partial EMT as the driver of tumor progression, iScience 24 (2021), 102113, https://doi.org/10.1016/j.isci.2021.102113.
[39] A. Dongre, M. Rashidian, E.N. Eaton, et al., Direct and indirect regulators of epithelial–mesenchymal transition– mediated immunosuppression in breast carcinomas, Cancer Discov. 11 (2021) 1286–1305, https://doi.org/10.1158/2159-8290.CD-20-0603.
[40] X. Liu, Y. Pu, K. Cron, et al., CD47 blockade triggers T cell–mediated destruction of immunogenic tumors, Nat. Med. 21 (2015) 1209–1215, https://doi.org/10.1038/nm.3931.
[41] T.A.W. Holderried, L. de Vos, E.G. Bawden, et al., Molecular and immune correlates of TIM-3 (HAVCR2) and galectin 9 (LGALS9) mRNA expression and DNA methylation in melanoma, Clin. Epigenet. 11 (2019) 161, https://doi.org/10.1186/s13148-019-0752-8.

[42] S. Yang, W. Wei, Q. Zhao, B7-H3, a checkpoint molecule, as a target for cancer immunotherapy, Int. J. Biol. Sci. 16 (2020) 1767–1773, https://doi.org/10.7150/ijbs.41105.
[43] E.A. Mesri, M.A. Feitelson, K. Munger, Human viral oncogenesis: a cancer hallmarks analysis, Cell Host Microbe 15 (2014) 266–282, https://doi.org/10.1016/j.chom.2014.02.011.
[44] J. Chen, S. Kendrick, Z. Qin, Mechanistic insights into chemoresistance mediated by oncogenic viruses in lymphomas, Viruses 11 (2019) 1161, https://doi.org/10.3390/v11121161.
[45] G. Herbein, Z. Nehme, Polyploid giant cancer cells, a hallmark of oncoviruses and a new therapeutic challenge, Front. Oncol. 10 (2020), 567116, https://doi.org/10.3389/fonc.2020.567116.
[46] I. Nečasová, M. Stojaspal, E. Motyčáková, et al., Transcriptional regulators of human oncoviruses: structural and functional implications for anticancer therapy, NAR Cancer 4 (2022), https://doi.org/10.1093/narcan/zcac005 zcac005.
[47] D. Jia, J.H. Park, H. Kaur, et al., Towards decoding the coupled decision-making of metabolism and epithelial-mesenchymal transition in cancer, Br. J. Cancer 124 (2021) 1902–1911.
[48] S.Y. Loo, L.P. Toh, W.H. Xie, et al., Fatty acid oxidation is a druggable gateway regulating cellular plasticity for driving metastasis in breast cancer, Sci. Adv. 7 (2021) eabh2443, https://doi.org/10.1126/sciadv.abh2443.
[49] H. Lv, G. Lv, C. Chen, et al., NAD+ metabolism maintains inducible PD-L1 expression to drive tumor immune evasion, Cell Metabol. 33 (2021) 110–127.e5, https://doi.org/10.1016/j.cmet.2020.10.021.
[50] W. Hua, P. ten Dijke, S. Kostidis, et al., TGFβ-induced metabolic reprogramming during epithelial-to-mesenchymal transition in cancer, Cell. Mol. Life Sci. 77 (2020) 2103–2123, https://doi.org/10.1007/s00018-019-03398-6.
[51] D. Wei, M. Xu, Z. Wang, J. Tong, The development of single-cell metabolism and its role in studying cancer emergent properties, Front. Oncol. 11 (2022), 814085, https://doi.org/10.3389/fonc.2021.814085.
[52] L. Yu, M. Lu, D. Jia, et al., Modeling the genetic regulation of cancer metabolism: interplay between glycolysis and oxidative phosphorylation, Cancer Res. 77 (2017) 1564–1574.
[53] D. Jia, B.B. Paudel, C.E. Hayford, et al., Drug-tolerant idling melanoma cells exhibit theory-predicted metabolic low-low phenotype, Front. Oncol. 10 (2020) 1426, https://doi.org/10.3389/fonc.2020.01426.
[54] T. Amemiya, T. Yamaguchi, Oscillations and dynamic symbiosis in cellular metabolism in cancer, Front. Oncol. 12 (2022), 783908, https://doi.org/10.3389/fonc.2022.783908.
[55] Z. Jiang, Z. Liu, M. Li, et al., Increased glycolysis correlates with elevated immune activity in tumor immune microenvironment, EBioMedicine 42 (2019) 431–442, https://doi.org/10.1016/j.ebiom.2019.03.068.
[56] A. Deshmukh, K. Deshpande, F. Arfuso, et al., Cancer stem cell metabolism: a potential target for cancer therapy, Mol. Cancer 15 (2016) 69, https://doi.org/10.1186/s12943-016-0555-x.
[57] S. Pasani, S. Sahoo, M.K. Jolly, Hybrid E/M phenotype(s) and stemness: a mechanistic connection embedded in network topology, J. Clin. Med. 10 (2020) 60, https://doi.org/10.3390/jcm10010060.